Journal of Materials Research and Technology, Volume 8, Issue 1, January–March 2019, pp. 703-712
DOI: 10.1016/j.jmrt.2018.05.016

Suppressing scratch induced brittle fracture in silicon by geometric design modification of the abrasive grits

Andrii M. Kovalchenko[a]*, Saurav Goel[b], Islam M. Zakiev [c], Evgeniy A. Pashchenko[d] and Rajab Al-Sayegh[e]

[a]Institute for Problems of Materials Science, National Academy of Sciences, Kyiv, 03142, Ukraine
[b]School of Aerospace, Transport and Manufacturing, Cranfield University, Bedfordshire, MK430AL, UK
[c]Institute of Superhard Materials, National Academy of Sciences, Kyiv, 04074, Ukraine
[d]National Aviation University, Kyiv, 03058, Ukraine
[e]College of Engineering, Northern Border University, Arar, 91431, Saudi Arabia

*Corresponding authors
E-mail address: and.kovalch@gmail.com (A.M. Kovalchenko)

Abstract:

The overarching goal of this research was to investigate the application of spherically shaped abrasive particles in achieving ductile-mode cutting. Scratching experiments were carried out to assess the differences between arbitrarily and spherically shaped diamond and tungsten carbide (WC) grits in inducing brittle fracture or ductile plasticity in single crystal silicon. It was observed that the arbitrarily shaped particles produce brittle fracture in contrast to the spherically shaped grits. The sharp edges and corners of grits result in high tensile stress concentrated regions causing cracking and spalling. Contrary to this, spherically shaped WC particles induce uniform cutting pressure, which suppresses the extent of the brittle fracture and the mode of material removal was completely dominated by ductile-cutting until a threshold load. These observations are expected to provide a suitable pathway in making the Diamond Wire Sawing process more robust by providing a control on brittle damage.

Keywords: Silicon; Diamond; Tungsten carbide; Ductile mode cutting; Scratching; Diamond wire sawing.

1. Introduction

Silicon has dominated the electronics and thereby the manufacturing industry for much of the 20th century, and the trend will continue in the upcoming years due to its enormous usage in photovoltaic solar cells, infrared optical elements, micro-circuits and micro-electro-mechanical systems. In a recent review, Wu [1] has highlighted that wafers of silicon are commercially produced by the Diamond Wire Sawing (DWS) process. The DWS process uses a steel wire coated or impregnated with diamond grits, which is fed into a silicon ingot. The cut surface of the silicon produced by the DWS process results in microcracks because of the brittle nature of silicon. Lapping, etching and Chemical Mechanical Polishing are major manufacturing steps extensively used to remove the surface damage (microcracks) occurring during the DWS process. This suggests that a

considerable incentive exists for achieving fully ductile mode cutting which will reduce the time and cost associated with post-sawing slurry laden processes.

Ductile-mode cutting of silicon is an established technology in which the ductile behaviour is realised by harnessing the pressure induced phase transformation in the deformation zone (diamond-structured cubic silicon transforms into the denser metallic β-tin structure). Upon release of the pressure, a transition to an amorphous phase has also been reported [2,3]. The theory of ductile plasticity exhibited by the brittle materials originated from the early indentation work of Lawn and Wilshaw [4] where the plasticity of brittle material under loading was observed and discussed. The possibility of machining brittle materials in the ductile-mode was then developed and proposed by Blake and Scattergood [5] and mathematical models to explain the importance of the crucial parameters leading to the ductile-brittle transition during single point diamond turning were proposed [6].

Numerous experimental and theoretical studies referred to in the review article [7] suggest that one of the critical parameters limiting the extent of the ductile-brittle transition in silicon during diamond machining is its critical undeformed chip thickness, the value of which depends on geometry of contact and machining conditions. The execution of ductile-mode cutting depends on parameters such as the crystallographic orientation of the silicon [8,9], temperatures [10-12], the presence and the type of lubricating liquid [13-16], and scratching speed [17,18]. What may however commonly be seen across all these studies is that a hydrostatic pressure of the phase transformation of silicon occurs in the pressure range of 10 to 16 GPa thereby bringing healthy plastic response in silicon [7,19]. If the pressure in the cutting zone is less than the critical threshold pressure, plasticity of silicon is not achievable. However, if the pressure is very high (more than 20 GPa), cracking occurs. Consequently, it has been realised that the processing window of ductile-regime machining is marginal, and failure to control the process may result in catastrophic brittle fracture dominated material removal.

A series of publications report investigations of ductile-mode removal of silicon in scratching depending on the geometry of the indenter. Gogotsi et al. [20] showed that only ductile removal was observed when a spherical (Rockwell) diamond tool was used, in contrast to the brittle fracture induced by sharp indenters (Vickers and conical). Wu and Melkote [21] demonstrated that scribers with a large tip radius produce lower tensile stresses and a higher degree of compression, that helps in achieving a larger critical depth of cut compared with scribers with a small radius. It was shown that spherically tipped scribers generate only surface cracks, while sharp tipped scribers (conical, Berkovich and Vickers) create large subsurface tensile stresses, which can lead to nucleation of subsurface cracks. Sumitomo et al. [22] showed that the tip with the smallest included angle resulted in the greatest scratching depths and the greatest material removal in the ductile regime.

In the studies reviewed above, the shape of the diamond tips investigated had a defined geometry (Rockwell, Vickers, etc.) whereas an industrial wire sawing operation uses arbitrarily shaped and randomly oriented abrasive grits. To mimic the wire sawing process, Würzner et al. [23] considered the role of surface structure in influencing the resulting substrate microcracks by scratching single diamond particle tips over the silicon substrate. Details of the shape, depth and distribution of the cracks have been obtained and discussed, however details about the ductile mode silicon removal were not considered. With this, Kumar et al. [24] have demonstrated the scribing of silicon by

abrasive grits on an actual diamond wire. Their results showed that the subsurface damage in silicon depends on the grit shape. While sharp grit produces chevron or radial cracks on the side of the groove that chipped out, round grit produces horseshoe-like cracks inside the groove. Kumar et al. [25] also have revealed the effects of using sharp-edged diamond wire grits. The progressive wear of the wire was observed to cause rounding and blunting of the abrasive diamond grits, and as a result the wafer surface morphology changed from brittle fracture to ductile cutting. A newly developed dicing wire saw was used in the experimental study of Suzuki et al. [26]. It was found that as the sawing cycle increased, the sharp tips of the diamond grits were rounded, leading to shallower/fewer saw marks and micro dents because of ductile mode slicing.

In view of the variation evident in the previously performed studies reviewed above, this study aims to perform a set of comparative scratching experiments by using irregular and well defined spherically shaped abrasive particles of diamond and tungsten carbide to observe the changes in the silicon removal phenomena, focusing on realisation of the ductile mode of material removal.

2. Methods

The scratching experiments were performed on a scratching machine (designed in-house) which permits gradual scaling of the load (increase or decrease) while recording friction force as a function of the displacement of a scriber. The schematic diagram of the testing rig is shown in Fig. 1. A customised scriber was prepared by depositing the abrasive particles onto a hardened steel ball made of bearing steel (AISI 52100, HRC 60). Three types of abrasive particles were used in the experiments: (i) diamond particles ranging in size from 28 to 40 μm, (ii) crushed tungsten carbide (WC) particles ranging in size from 25 to 50 μm and (iii) round tungsten carbide (WC) particles ranging in the size from 35 to 45 μm. The scanning electron microscopy (SEM) images of the abrasive particles are shown in Fig. 2.

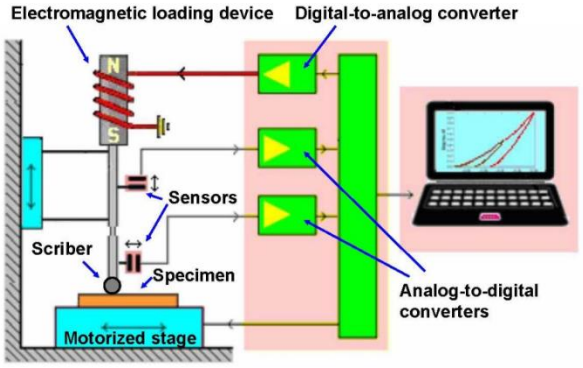

Fig. 1 – The schematic diagram of the scribing testing rig.

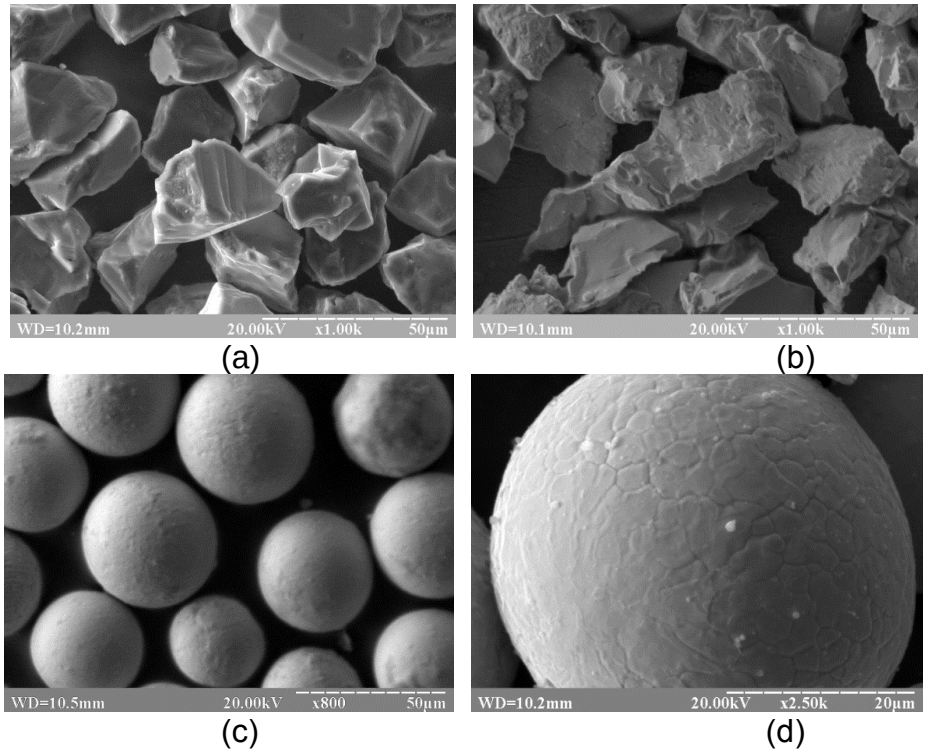

Fig. 2 – SEM images of (a) abrasive diamond particles, (b) crushed tungsten carbide particles, (c) spherical tungsten carbide particles and (d) higher magnification image of the single WC particle.

One major reason for choosing tungsten carbide (WC) for scratching the silicon was because of its superior scratch hardness (WC has Mohs hardness of about 9 while silicon has Mohs hardness of 6 to 7). The second reason of using WC was to achieve a perfect spherical shape which is difficult to achieve in diamond grits because of diamond's hard anisotropic cutting directions. Spherical WC particles were produced using plasma thermal centrifugal spraying technology. Dzykovich et al. [27] have described in detail the fabrication and the mechanical properties of such tungsten carbide particles. After spraying, the WC particles were separated from wide fraction ranging from 10 to 300 µm to the narrow sizes studied by sedimentation in liquid under the action of centrifugal force. The particles were made to hold on to the steel ball (Ø 4 mm) surface using epoxy resin which is a typical practice followed in fabricating diamond cutting tools as well. The scribing was performed along the [110] crystallographic direction on the (100) surfaces of monocrystalline mirror-polished microelectronic grade silicon rectangular plate (4×2 cm). A constant scribing speed of 20 µm/s with a total scribing length of 3 mm was adopted for the purposes of experimentation. The load function was programmed with an initial gradual increase of normal load up to 1 N, reached half way along the scribing length; and a gradual decrease of the load to 0 N by the end of scratch. The tests with each type of abrasive particles were repeated 3 times. After scribing, the resulting surface morphology was studied using a SEM and optical profilometry.

3. Results and discussions

The plots of the friction force as well as the SEM images of the scratched tracks recorded in three test cases; (i) scribing performed using diamond grits, (ii) scribing performed using arbitrarily shaped WC particles and (iii) scribing performed using spherically shaped WC particles are shown in Fig. 3a-c, Fig. 4a-b and Fig. 5a-b respectively.

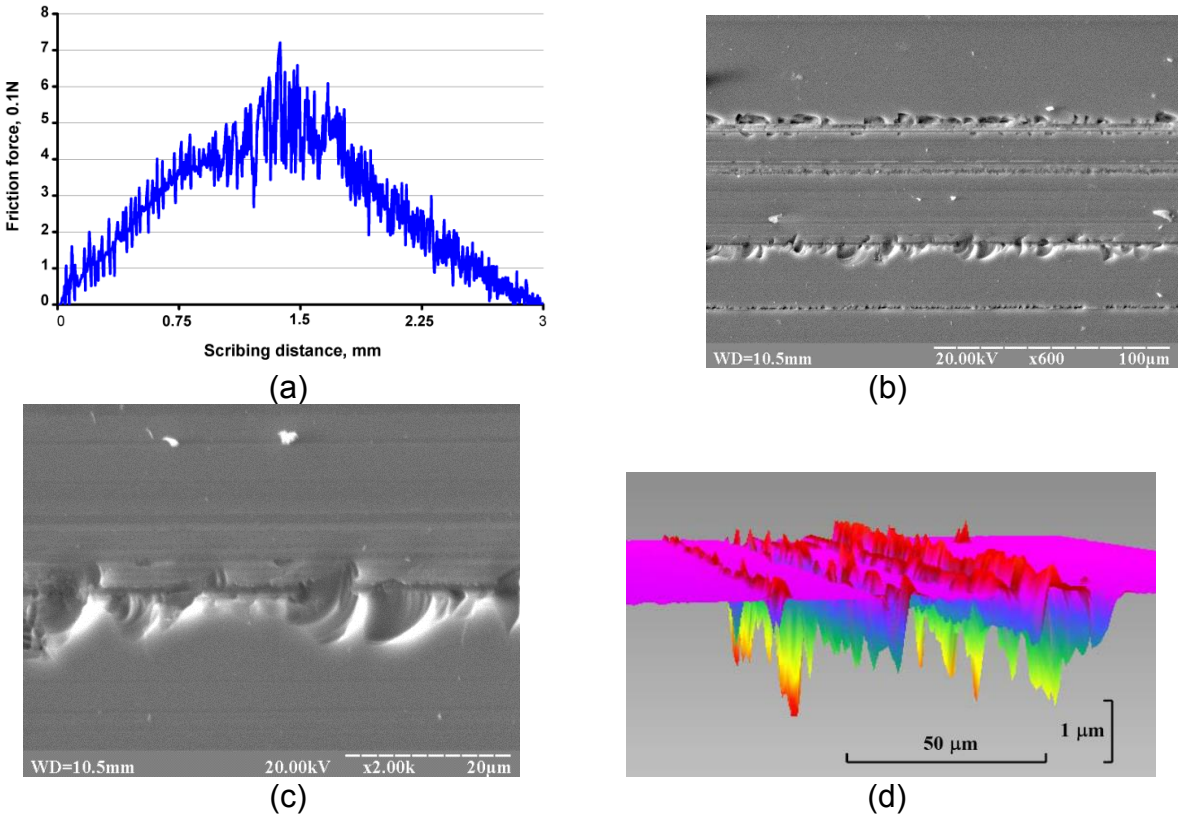

Fig. 3 – Experimental data of (a) friction force, (b) corresponding SEM images of the scratches made in silicon using **arbitrarily shaped diamond particles**, (c) the magnified fragment from the area (b) showing the scratches with brittle damage (in the center) and small/very small/extremely small ductile scratches in the upper and lower part of the photo. Three dimensional (3D) optical profilometry image (d) of the scratched area.

During scratching of silicon using arbitrarily shaped diamond particles, as evident from Fig. 3a, the friction force showed continuous vibration with a monotonic increase until the midpoint of the scratch, and a corresponding decrease in the second half of the scratch. The continuous vibrations in the friction force are suggestive of the occurrence of brittle conchoidal fracture alongside ductile deformation during the scratch. SEM observation of the scratched areas reveals that the diamond particles produce a few sharp parallel scratches on the silicon surface. The scratches shown in Fig. 3b-c can be divided into two groups; (i) deeper scratches revealing marks of brittle fracture (these scratches are clearly recognised in lower magnification images), (ii) smaller scratches where silicon has deformed in a purely ductile mode which are particularly visible in the fragment of Fig. 3c. Alongside brittle fracture, the ploughing of the ductile material may also be seen in

scratches where the brittle mode fracture was dominant, seen in Fig. 3c. Also, the marks of brittle fracture seen in the case of the deeper scratches extend along the entire length of the scratch. Optical profilometry observation demonstrates that the depth of brittle fracture extends up to 2 μm (Fig. 3d).

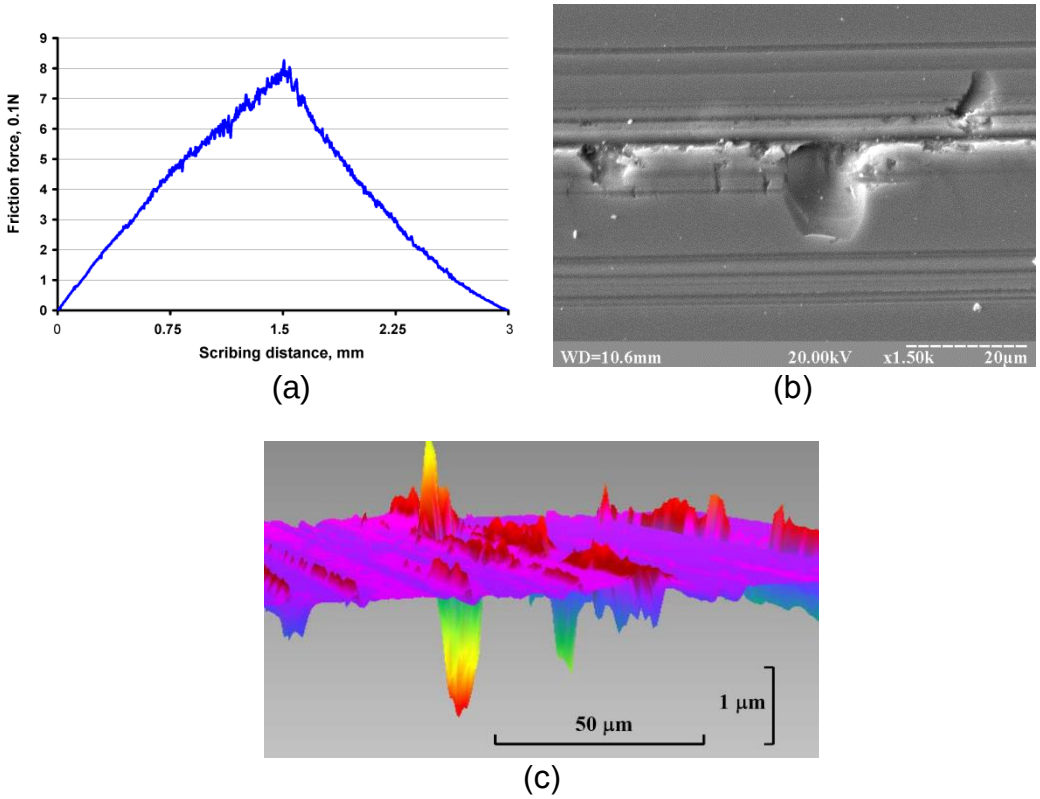

(a) (b)

(c)

Fig. 4 – Experimental data of (a) friction force and (b) corresponding SEM image of the area scratched in silicon using **crushed WC particles.** 3D optical profilometry image (c) of the scratched area.

In Fig. 4, the observation of the cracking noise and the extent of brittle fracture can be seen to reduce when using arbitrarily shaped WC particles in comparison to arbitrarily shaped diamond grits seen earlier in Fig. 3. The vibration on the record of friction force (Fig. 4a) was observed to be limited to the midpoint of the scratch. Although, Fig. 4b highlights the occurrence of brittle fracture, the spalling areas in the sides of some scratches are smaller than what is seen in Fig. 3b-c (scratching made with arbitrarily shaped diamond particles). Most single scratches on the scribing track, especially at the sides of the track and at the beginning and at the end of the scribing path, were formed in the ductile mode (Fig. 4b). Optical profilometry of the scratched area also demonstrates a reduction in the extent of brittle fracture caused by the WC crushed particles (Fig. 4c) in comparison with the diamond grits despite the depth of some brittle spalled areas being around 2 μm. At this stage, it is postulated that the lesser extent of brittle fracture relates to the lower mechanical strength of tungsten carbide and the lower sharpness of the edges and corners of the crushed tungsten carbide particles (see Fig. 2a,b) thereby inducing less contact pressure compared to diamond grits.

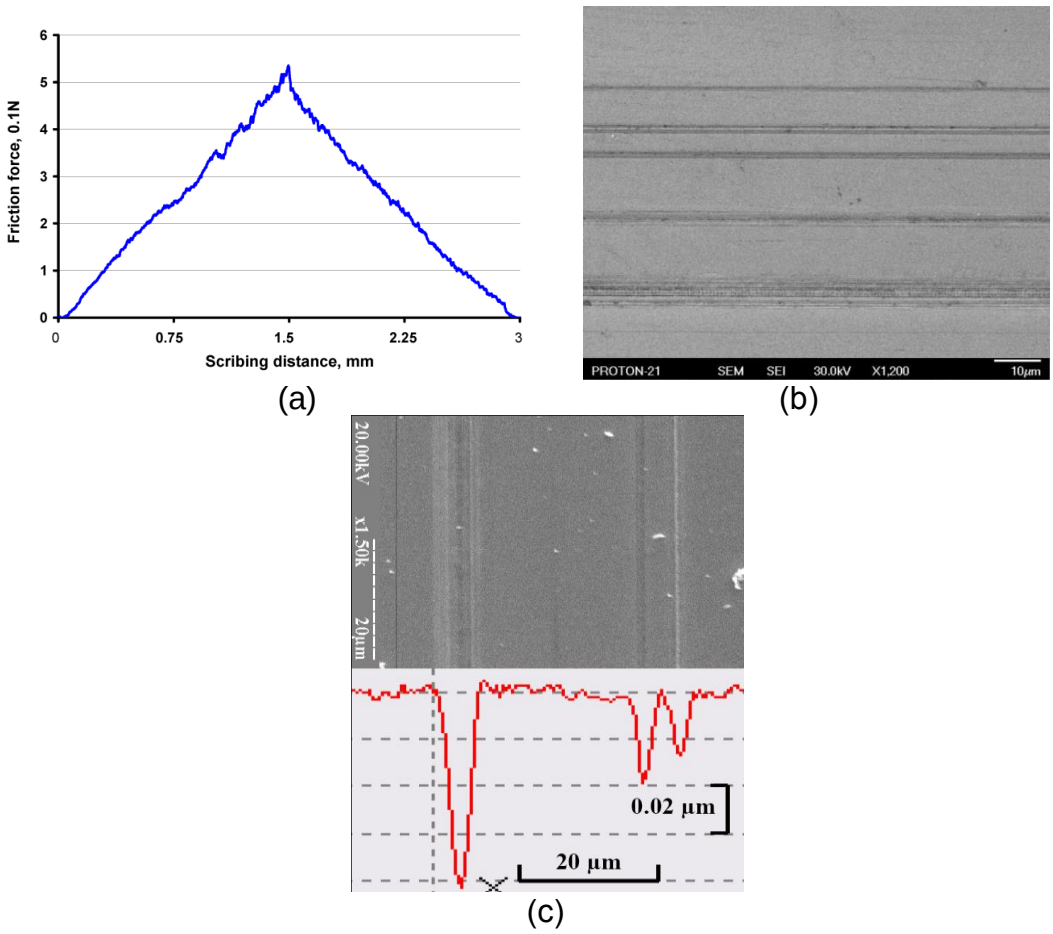

Fig. 5 – Experimental data of (a) friction force, (b) the SEM image of the area scratched in silicon using **spherically shaped WC particles** and (c) the SEM fragment with a few scratches and corresponding two-dimensional profile.

In the third case where spherically shaped WC particles were used (Fig. 5a), the cracking noise and the vibrations were absent in the record of the friction force. Scratches were very smooth and no cracking was observed on or near the scratched surface (Fig. 5b). From this observation it can be deduced that the ductile-to-brittle transition in silicon during the scratching experiments while using a normal load of 1 N was inhibited by using the spherically shaped WC grits, however, only a shallow depth of scratch was obtained (up to 80 nm). The transverse profiles of a few scratches are shown in Fig. 5c. In fact, the transverse sections of the grooves correspond only to the trajectories of the moving penetrated spherical tungsten carbide particles (horizontal projection) below the silicon surface. Also, no damage was observed on the spherical tungsten carbide particles post-scratching.

From the experimental observations we infer that the contact pressure under the spherical WC particles reached the value of the pressure of phase transformation but that the maximal normal load of 1 N in the present experimental conditions was not sufficient to reach the critical contact pressure of the ductile-to-brittle transition when the cracks appeared. Despite this, estimation of the exact load acting on each particle and the contact

pressure underneath each grit is challenging in our case due to the unevenness in the distribution of the WC particles on the steel ball indenter i.e. bigger grits protuberate more than the smaller particles, and it is these bigger protuberated particles that cause most of the material removal. Evaluation of the exact load acting on a single particle and the corresponding contact pressure underneath individual grits is more suitable to be carried out bysimulation, such as molecular dynamics demonstrated by Goel et al. [28] or finite element analysis by Rashid et al. [29]. However, in one of our experiments, favorable conditions appeared that made it possible to estimate the contact pressure underneath a grit. It was the rare case when only one individual particle contacted silicon producing a single groove enabling us to estimate contact conditions with known values of normal load, friction force and contacting area.

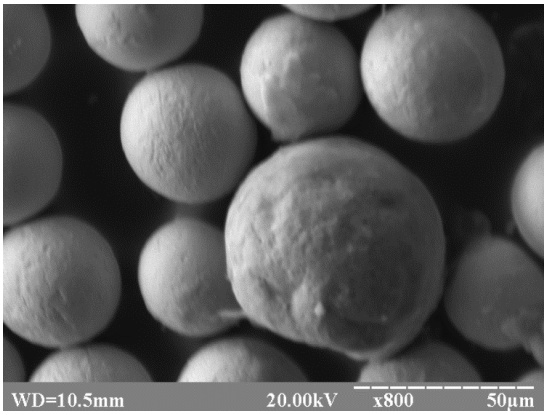

Fig. 6 – Post-SEM image of the spherical tungsten carbide particles (largest particle has 60 µm in diameter which produced single scratch on the silicon plate).

Fig. 6 shows a post-scratching SEM image of the spherical WC particles wherein the largest particle was observed to have a diameter of 60 µm. It was observed during the experiments that this largest diameter particle protuberated more than the other particles. It allowed a homogeneous contact between the WC particle and the silicon substrate during the scratching process. The presence of this bigger WC particle among other particles having sizes varying between 35 and 45 µm is expected to be due to the lower density of the particle's material formed during solidification after spraying. Despite the bigger size and lower density, the weight of the particle is in the same range as the other smaller particles. It is believed that the weight of the particle is the main parameter influencing the separation during sedimentation in liquid under the action of centrifugal force. Therefore, this particle could not be removed from the main particles' fraction with smaller sizes.

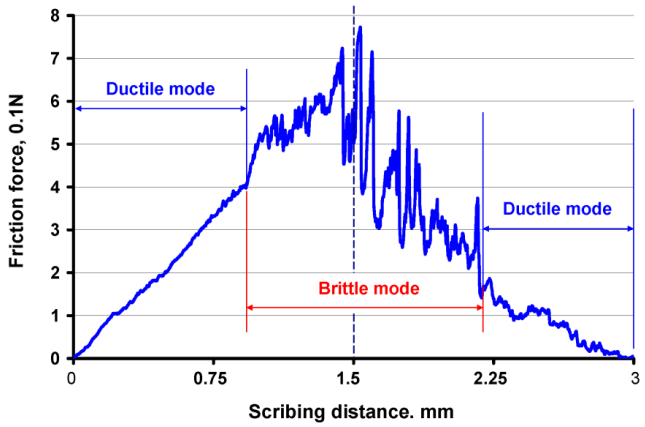

Fig. – 7 Variation in the friction force while scratching with a single tungsten carbide spherical particle (Ø 60 µm).

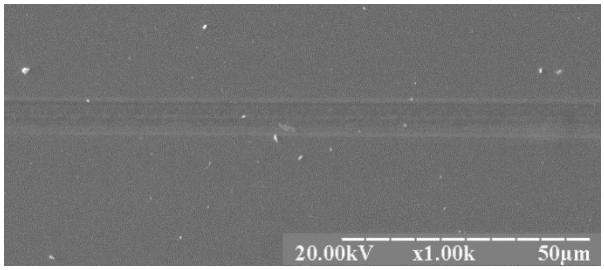

(a)

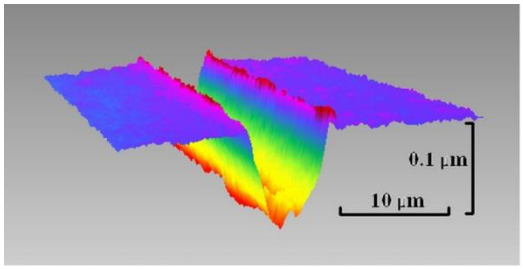

(b)

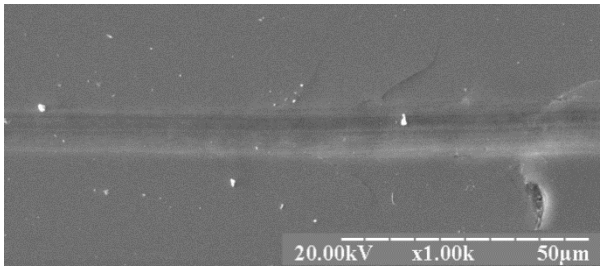

(c)

Fig. – 8 SEM image of the scratched silicon surface scribed by a single tungsten carbide grit (a) in ductile mode at the beginning of the scratch, (b) corresponding optical three-dimentional image and (c) SEM image at a scratch distance of 0.9 mm from the beginning of movement where the first cracks appeared.

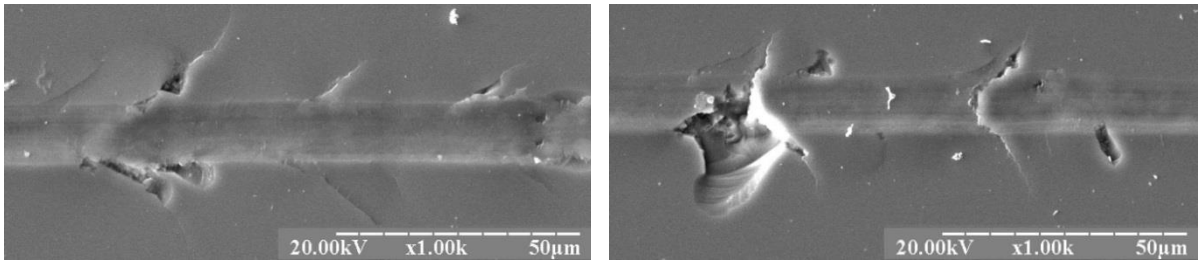

(a) (b)

Fig. – 9 SEM images (a,b) of the central part of the scratch on silicon made using the spherically shaped single tungsten carbide grit (∅ 60 µm), revealing cracking and spalling.

Fig. 7 shows the record of friction force wherein Figs. 8 and 9 show the post-scratch SEM images of silicon obtained from the scratch made by the spherical WC particle (Ø 60 µm). It is evident from Fig. 8 that the ductile-mode material removal was achieved at the beginning of the scratching length, up to 0.9 mm along it. Optical profilometry observation clearly confirms the ductile behaviour of the material. Fig. 8b shows a 3D optical image of the scratch taken in the zone of ductile mode material removal, highlighting the formation of pop-up hillocks from the deformed materials at the edges of the scratch. The record of friction force in Fig. 7 confirms that the cracking was fully absent and that the friction force increases smoothly with the increase of the normal load. The first crack appeared after 0.9 mm of scratching length where the normal load reached 0.6 N, and tangential friction force was 0.4 N (Fig. 7). From this point, the friction force rose sharply and began to fluctuate with characteristic cracking noise. Consequently, median cracks emerge on the sides of the scratch, ultimately leading to spalling at the maximal normal load at the centre of the scratch. The cracks and spalling observed in the midpoint of the scratch are shown in Fig. 9. The friction force in this region was very unstable, with significant noise. Apparently, there was a noticeable increase in the friction force during the deformation due to a concentrated increase in the fracture stress (σ_f) beyond the critical value of fracture toughness (K_c) (for silicon it's about 1 $MPa.m^{1/2}$) which causes the appearance of the cracks and spalling. After cracking, the stresses in the material drop, as shown by the sharp drop in the friction force. Also, the process was seen to exhibit a periodical character, i.e. the occurrence of cracks and spalling along the scratch length occurs periodically as shown in some post-scratching snapshots in Fig. 9a,b. It is interesting that the scratching done by the spherical WC particle at maximal normal load is not purely brittle. The main portion of the scratch has a typical ductile appearance (Fig. 9a,b). This scratching mode performed by the WC particles contrasts with the scratches performed by the diamond particles, which showed the spalled areas to be of a continuous type (Fig. 3b,c). However, the extent of this cracking and spalling decreases in the second half of the scratch with the decreasing normal load. The last cracks and spalling were observed at the distance 2.18 mm from the beginning of the scratch, where the normal load was 0.55 N and the friction force was less than 0.2 N, which implies the reverse transition from brittle mode to pure ductile mode scratching. Beyond this point up to the end of the scratch (normal load < 0.55 N), the scratch obtained was very smooth in nature, like in the beginning of the scratch. Also, the slope of the friction force in the ductile mode cutting during the unloading regime was less steep than in the ductile regime material removal during the loading stage (Fig. 7). Such differences observed during the loading

and unloading stages can arise from the differences in the contact area, i.e. an increase in the contact area due to the damage of the contacting surface of the WC particle (see Fig. 6) results in a homogenous stress distribution.

The critical stress of ductile-to-brittle transition could be estimated with knowledge of the diameter of the single spherical WC particle, the actual load and depth of cut at the point of the first cracks appearance. However, the exact mathematical calculation could not be performed due to the rather complicated mechanism of the plastic deformation of silicon during scratching and subsequent crack initiation. The images of the area and the cross-sectional profile at the point just before the first small crack (indicated by the arrows) are shown in Fig. 10. As evident, the level of deformation leading to the material pile up and side flow was significantly increased compared to the aforementioned area of the scratch shown in Figs. 8(a,b). The elevation of the deformed material above the initial flat silicon surface is clearly seen in the profile A-A when the small inner cracks (inside the scratch) are recognized in the longitudinal profile B-B (Fig.10d).

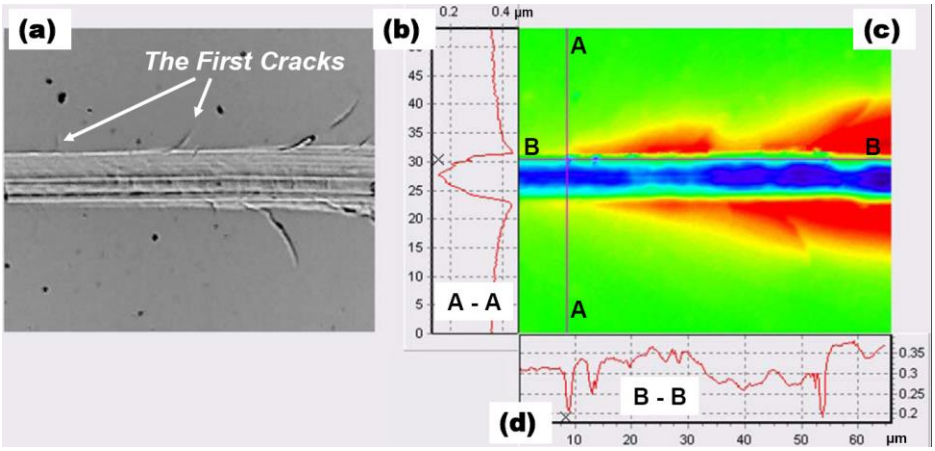

Fig. – 10 The optical image of the scratch in the area of the first cracks appearance (indicated by arrows) (a), the profile of the scratch cross-section just in the beginning of cracking (b), two-dimensional image displaying the horizontal level of lifting material by different colors (c) and longitudinal profile of the side line in the scratch (d). The vertical line A-A and horizontal line B-B in figure (c) indicate the location of the measured profile in figure (b) and (d). The area corresponds to SEM image in Fig. 8c.

We assume that the contact pressure for the initiation of brittle fracture has reached the critical value in the point where the first crack is observed. This location corresponds to the line A-A in Fig. 10(c). A diagram of a single tungsten carbide particle scratching against silicon, accounting for the deformation in front of and alongside the particle is shown in Fig. 11a. To estimate the contact area between the spherical particle and the deformed silicon during scratching (the particle ploughs through the silicon), we assume that the height of the wedge from the plastic material in front of the moving particle is about the same as the elevation of the deformed material along the side of the scratch (Fig. 11b).

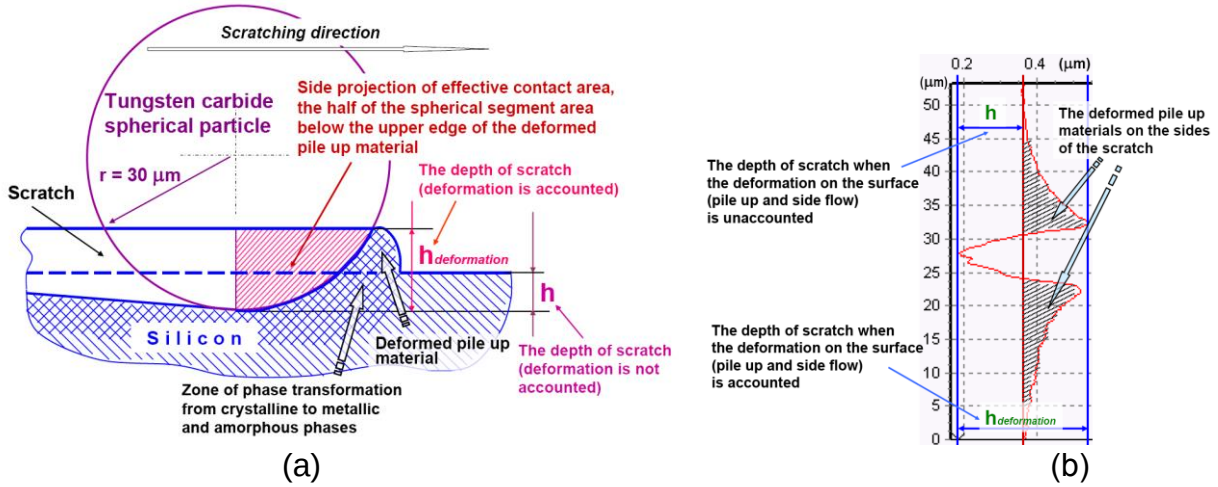

Fig. – 11 Diagram of a single spherical tungsten carbide particle scratching against silicon, showing the estimation of depth of the scratch accounting the wedge formation in front of the particle (a) and the transversal profile of the scratch (b) showing the estimation of depth of the scratch accounting the plastic deformation alongside the scratch ($\mathbf{h_{deformation}}$) and without accounting the plastic deformation (**h**). Note that the actual relative dimensions of the particle and the depth of scratch are differing from the diagrams.

At the point of the cracking initiation (line A-A in the Fig. 10c), the depth of the scratch accounting for the deformation ($\mathbf{h_{deformation}}$) is equal to 0.25 µm, the depth of the scratch without accounting for the plastic deformation (**h**) is equal to 0.17 µm. Knowing these values and the diameter of the WC particle (we consider that the curvature of the scratch is equal to the curvature of the spherical WC particle) it is possible to calculate the effective contact area which is the front half area of the spherical segment with height equal to the objective depth of scratch ($\mathbf{h_{deformation}}$) (Fig. 11). The contact pressure may be estimated using the values of the applied normal load and the projected contact area. The calculation of average contact pressure is presented as extract information in the **Appendices**. The average pressure, accounting for the material deformation, according to the calculation is around 25 GPa. The calculation of the average contact pressure without accounting for the material deformation and the wedge formation in front of the particle, where the depth of scratch is only the depth of the particle penetration through the silicon (see Fig. 11) isabout 37 GPa. This value is apparently well above the theoretical estimates made for predicting cracks in silicon. According to the experimental work of Gridneva et al. [30] and the molecular dynamics simulation based studies of Goel et al. [19], as well as finite element calculation of Yan et al. [31], the required yielding stresses or contact pressure estimated for the occurrence of phase transition in silicon to cause plasticity is in the range of 10 to 16 GPa. An increase in the value of stress beyond this value causes concentration of stress in a confined volume, thus causing crack initiation. The experimental and theoretical studies referred to in the review paper [7] indicates that crack propagation occurs when the stresses attain a certain critical value, in the majority of cases about 20 GPa in the birthplaces of cracks. From the aforementioned discussion, the calculation of the contact pressure accounting for the plastic deformation is more applicable to our case.

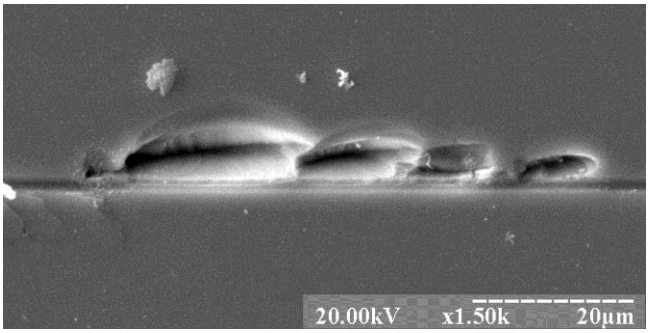

Fig. – 12. The cavities produced by the pulled-out rotating crushed tungsten carbide particle outside of the ductile scratched groove.

Another cause of the crack's appearance is the broken continuity between the particles and the resin i.e. insufficient strength of the binding epoxy resin that occurs occasionally during scratching experiments, resulting in the loose entrapment of such particles between the moving pin and the silicon, which produces brittle damage. Fig. 12 shows the brittle cavities produced by the pulled-out rotating crushed tungsten carbide particle outside of the scratched groove. It may be noted that all three types of particle studied in this work produced brittle damage after detachment from the steel ball and the resulting brittle damage was diverse in form; different lateral and median cracks as well as pits and cavities were observed. Kumar et al. [25] noticed that the same brittle damage was produced by the occasional indenting action of loose diamond abrasives dislodged from the actual diamond wire, confirming the hypothesis proposed in this work.

Conclusions

Comparative studies were carried out to observe the difference between arbitrarily shaped and spherically shaped grits of diamond and tungsten carbide respectively during scratching of single crystal silicon under the same loading conditions (maximum normal load of 1 N).

The use of arbitrarily shaped particles causes the material removal mode to be predominantly brittle fracture. However, under the same loading conditions, a fracture free (completely ductile) regime of material-removal was obtained by using smooth, spherically shaped WC particles. These observations explain that the sharp edges and corners of diamond and crushed WC particles induce fracture stress beyond the critical value of fracture toughness causing cracks and spalling.

Spherically shaped WC particles induce uniform pressure, which suppress the extent of the brittle fracture and the mode of material removal was completely dominated by ductile-cutting until a threshold load. However, depths of scratches in the ductile mode are significantly lower than depths of brittle scratches. Depths of ductile scratches are in the same range as the penetrating abrasive particle, in contrast with brittle scratches where the depths of scratches extend deeper, covering the diapason of brittle spalling of silicon.

Appendices

Past literature describes that the mean contact pressure (p_m) or scratch hardness exerted by the abrasive grit (WC particle) on to the substrate (silicon) [32] can be obtained from the ratio of the applied normal load and the projected contact area. The value of normal force during scratching is straightforward, however, the calculation of the projected contact area present complications. We have examined two scenarios as follows based on which final inference was drawn that the mean contact pressure during scratching of silicon with WC was about **25 GPa**:

Case 1: Depth of scratch calculations neglecting pile up and side flow

Table A.1

Normal Force (N)	Radius of the WC grit (r)	Depth of scratch (h)	Total projected area ($2\times\pi\times r\times h$)	Effective projected area = Total projected area/2 (since only ½ of the ball area contact silicon)	Mean contact pressure (p_m) = Normal force / effective projected area
0.6 N	30 µm	**0.17 µm**	3.2×10^{-11} m^2	1.6×10^{-11} m^2	**37.45 GPa**

Calculated mean contact pressure (p_m) = 37.45 GPa
Uniaxial yielding stress (σ_y) of silicon = 12.32 GPa [19]
Ratio of p_m / σ_y = **3.04**

Case 2: Depth of scratch calculations include pile up and side flow

Table A.2

Normal Force (N)	Radius of the WC grit (r)	Depth of scratch ($h_{deformation}$)	Total projected area ($2\times\pi\times r\times h_{deformation}$)	Effective projected area = Total projected area/2 (since only ½ of the ball area contact silicon)	Mean contact pressure (p_m) = Normal force / effective projected area
0.6 N	30 µm	**0.25 µm**	4.71×10^{-11} m^2	2.356×10^{-11} m^2	**25.46 GPa**

Calculated mean contact pressure (p_m) = **25.46** GPa
Uniaxial yielding stress (σ_y) of silicon = 12.32 GPa [19]
Ratio of p_m / σ_y = **~2**

It is documented [33] that for an ideal plastic contact, the ratio of mean contact pressure (p_m) and yielding stress (σ_y) of the material should be between 1.5 to 2. From a comparison

of Case 1 and Case 2, it is clear that the depth of scratch calculations performed by including pile up and side flow revealed the mean contact pressure (p_m) to be **25.46 GPa** also satisfying the criterion proposed in the literature.

References

[1] Wu H. Wire sawing technology: A state-of-the-art review. Precis Eng 2016;43:1–9.
[2] Domnich V, Gogotsi Y. 5. High-pressure surface science. In: Nalwa HS, editor. Handbook of Surfuces and Interfaces of Materials. Academic Press; 2001, p. 195–237.
[3] Goel S, Luo X, Agrawal A, Reuben RL. Diamond machining of silicon: a review of advances in molecular dynamics simulation. Int J Mach Tools Manuf 2015; 88:131–164.
[4] Lawn B, Wilshaw R. Indentation fracture: principles and applications. J Mater Sci 1975; 10(6):1049–81
[5] Blake PN, Scattergood RO. Ductile-regime machining of germanium and silicon. J Am Ceram Soc 1990;73(4): 949–57.
[6] Morris JC, Callahan DL, Kulik J, Patten JA, Scattergood RO. Origins of the ductile regime in single-point diamond turning of semiconductors. J Am Ceram Soc 1995;78(8):2015–20.
[7] Kovalchenko AM. Studies of the ductile mode of cutting brittle materials (A review). J Superhard Mater 2013;35(5):259–76.
[8] O'Connor BP, Marsh ER, Couey JA. On the effect of crystallographic orientation on ductile material removal in silicon. Precis Eng 2005;29(1):124–32.
[9] Jasinevicius RG, Duduch JG, Montanari L, Pizani PS. Dependence of brittle-to-ductile transition on crystallographic direction in diamond turning of single-crystal silicon. Proceedings of the Institution of Mechanical Engineers, Part B: J Eng Manuf 2012;226(3):445–58.
[10] Okabe H, Tsumura T, Shimizu J, Zhou LB, Eda H. Experimental and simulation research on influence of temperature on nano-scratching process of silicon wafer. Key Eng Mater 2007;329:379–84.
[11] Smith JF, Zheng S. High temperature nanoscale mechanical property measurements. Surf Eng 2000;16(2):143–46.
[12] Zarudi I, Nguyen T, Zhang LC. Effect of temperature and stress on plastic deformation in monocrystalline silicon induced by scratching. Appl Phys Lett 2005;86(1):011922.
[13] Li X, Lu J, Wan Z, Meng J, Yang S. A simple approach to fabricate amorphous silicon pattern on single crystal silicon. Tribol Int 2007;40(2):360–64.
[14] Danyluk S, Reaves R. Influence of fluids on the abrasion of silicon by diamond. Wear 1982;77(1):81–7.
[15] Yu B, Qian L, Dong H, Yu J, Zhou Z. Friction-induced hillocks on monocrystalline silicon in atmosphere and in vacuum. Wear 2010;268(9):1095–1102.
[16] Kumar A, Melkote SN. The chemo-mechanical effect of cutting fluid on material removal in diamond scribing of silicon. Appl Phys Lett 2017;111(1):011901.
[17] Gassilloud R, Ballif C, Gasser P, Buerki G, Michler J. Deformation mechanisms of silicon during nanoscratching. Physica Status Solidi (a) 2005;202(15):2858–69.
[18] Zhang Z, Wang B, Kang R, Zhang B, Guo D. Changes in surface layer of silicon wafers from diamond scratching. CIRP Annals-Manuf Technol 2015;64(1):349–52.
[19] Goel S, Kovalchenko A, Stukowski A, Cross G. Influence of microstructure on the cutting behaviour of silicon. Acta Mater 2016;105:464–78.

[20] Gogotsi Y, Zhou G, Ku SS, Cetinkunt S. Raman microspectroscopy analysis of pressure-induced metallization in scratching of silicon. Semicond Sci Tech 2001;16(5):345–52.
[21] Wu H, Melkote SN. Study of ductile-to-brittle transition in single grit diamond scribing of silicon: application to wire sawing of silicon wafers. J Eng Mater Technol 2012;134(4):041011.
[22] Sumitomo T, Huang H, Zhou L. Deformation and material removal in a nanoscale multi-layer thin film solar panel using nanoscratch. Int J Mach Tool Manuf 2011;51(3):182–9.
[23] Würzner S, Buchwald R, Retsch S, Möller HJ. Investigation of the development of the microcrack structure in scratch tests with single diamond particles on monocrystalline silicon wafers. In: Proceedings of the 29th European Photovoltaic Solar Energy Conference and Exhibition (EU PVSEC 2014); 2014 September; Amsterdam, The Netherlands; p. 22-26.
[24] Kumar A, Melkote SN, Kaminski S, Arcona C. Effect of grit shape and crystal structure on damage in diamond wire scribing of silicon. J Am Ceram Soc 2017;100(4):1350–59.
[25] Kumar A, Kaminski S, Melkote SN, Arcona C. Effect of wear of diamond wire on surface morphology, roughness and subsurface damage of silicon wafers. Wear 2016; 364:163–8.
[26] Suzuki T, Nishino Y, Yan J. Mechanisms of material removal and subsurface damage in fixed-abrasive diamond wire slicing of single-crystalline silicon. Precis Eng 2017;50;32–43.
[27] Dzykovich VI, Zhudra AP, Bely AI. Properties of tungsten carbide powders produced by different technologies. The Paton Welding J 2010;4:22–4.
[28] Goel S, Faisal NH, Luo X, Yan J, Agrawal A. Nanoindentation of polysilicon and single crystal silicon: molecular dynamics simulation and experimental validation. J Phys D: Appl Phys 2014;47(27):275304.
[29] Rashid WB, Goel S, Luo X, Ritchie JM. The development of a surface defect machining method for hard turning processes. Wear 2013;302(1):1124–35.
[30] Gridneva IV, Milman YV, Trefilov VI. Phase transition in diamond-structure crystals during hardness measurements. Physica status solidi (a) 1972;14(1):177–82.
[31] Yan J, Zhao H, Kuriyagawa T. Effects of tool edge radius on ductile machining of silicon: an investigation by FEM. Semicond Sci Tech 2009;24(7):075018.
[32] Pelletier H, Gauthier C, Schirrer R. Friction effect on contact pressure during indentation and scratch into amorphous polymers. Mater Letters 2009;63(20):1671–1673.
[33] Paar SCA, de Segurança D, Corporativa E. In-situ observation of the scratch/indentation true contact area to provide analysis without being model-dependent. Available from: https://www.azom.com/article.aspx?ArticleID=13986